

# NASA TECHNICAL MEMORANDUM



NASA TM X-3171

NASA TM X-3171

(NASA-TM-X-3171)	ANALYSIS OF NOISE PRODUCED	N75-15399
BY JET IMPINGEMENT NEAR THE TRAILING EDGE OF		
A FLAT AND A CURVED PLATE (NASA)	32 p HC	
\$3.75	CSSL 20A	Unclas
		H1/71 07806

## ANALYSIS OF NOISE PRODUCED BY JET IMPINGEMENT NEAR THE TRAILING EDGE OF A FLAT AND A CURVED PLATE

*Daniel J. McKinzie, Jr., and Robert J. Burns*

*Lewis Research Center  
Cleveland, Ohio 44135*



1. Report No. NASA TM X-3171	2. Government Accession No.	3. Recipient's Catalog No.	
4. Title and Subtitle ANALYSIS OF NOISE PRODUCED BY JET IMPINGEMENT NEAR THE TRAILING EDGE OF A FLAT AND A CURVED PLATE		5. Report Date January 1975	6. Performing Organization Code
		8. Performing Organization Report No. E-8080	10. Work Unit No. 505-03
7. Author(s) Daniel J. McKinzie, Jr., and Robert J. Burns		11. Contract or Grant No.	
9. Performing Organization Name and Address Lewis Research Center National Aeronautics and Space Administration Cleveland, Ohio 44135		13. Type of Report and Period Covered Technical Memorandum	
		14. Sponsoring Agency Code	
12. Sponsoring Agency Name and Address National Aeronautics and Space Administration Washington, D. C. 20546		15. Supplementary Notes	
16. Abstract The sound fields produced by the interaction of a subsonic cold gas jet with the trailing edge of a large flat plate and a curved plate were analyzed. The analyses were performed to obtain a better understanding of the dominant noise source and the mechanism governing the peak sound-pressure-level frequencies of the broadband spectra. An analytical expression incorporating an available theory and experimental data predicts sound field data over an arc of approximately $105^\circ$ measured from the upstream jet axis for the two independent sets of data. The dominant noise as detected on the impingement side of either plate results from the jet impact (eighth power of the velocity dependence) rather than a trailing-edge disturbance (fifth or sixth power of the velocity dependence). Also, the frequency of the peak SPL may be governed by a phenomenon which produces periodic formation and shedding of ring vortices from the nozzle lip.			
17. Key Words (Suggested by Author(s)) Jet noise; Impingement noise; Impact noise; Jet flat-plate impact; STOL aircraft noise; EBF noise		18. Distribution Statement Unclassified - unlimited STAR category 71 (rev.)	
19. Security Classif. (of this report) Unclassified	20. Security Classif. (of this page) Unclassified	21. No. of Pages 31	22. Price* \$3.75

\* For sale by the National Technical Information Service, Springfield, Virginia 22151

# ANALYSIS OF NOISE PRODUCED BY JET IMPINGEMENT NEAR THE TRAILING EDGE OF A FLAT AND A CURVED PLATE

by Daniel J. McKinzie, Jr., and Robert J. Burns

Lewis Research Center

## SUMMARY

The sound fields produced by the interaction of a subsonic cold gas jet with the trailing edge of a large flat plate and a curved plate were analyzed. The analyses were performed to obtain a better understanding of the dominant noise source and the mechanism governing the peak sound-pressure-level frequencies of the broadband spectra. An analytical expression incorporating an available theory and experimental data predicts sound field data over an arc of approximately  $105^\circ$  measured from the upstream jet axis for the two independent sets of data. Results indicate that the noise from either plate emanates from two principal sources, the impact of the jet on the plate and the flow over the plate's trailing edge. At jet Mach numbers above 0.5, the dominant noise as detected on the impingement side of either plate results from the jet impact (eighth power of the velocity dependence) rather than a trailing-edge disturbance (fifth or sixth power of the velocity dependence). Also, the frequency of the peak SPL may be governed by a phenomenon which produces periodic formation and shedding of ring vortices from the nozzle lip.

## INTRODUCTION

For adequate lift augmentation in the externally blown flap (EBF) concept of the short takeoff and landing (STOL) aircraft, the engine exhaust is deflected downward during takeoff and approach by a wing with flaps. The impingement of the jet on the flap surfaces results in considerable additional noise above that produced by the jet alone (refs. 1 and 2).

The interaction noise produced by the impingement of the jet against the flaps of the EBF STOL aircraft is generally considered to result from several major sources. References 2 to 4, which consider a two-flap EBF configuration, have described the dominant interaction noise sources as leading-edge noise, scrubbing noise, and trailing-edge noise. Reference 5, which considers a three-flap configuration, presents a detailed

account of the noise sources. A study of the flap surface pressure fluctuations in the approach setting ( $15^\circ$ ,  $35^\circ$ ,  $50^\circ$  flaps) revealed generally higher fluctuating pressure levels than for the takeoff flap setting ( $0^\circ$ ,  $20^\circ$ ,  $40^\circ$ ), and the highest levels appeared near the trailing edges. The third flap ( $50^\circ$ ) was subjected to the highest pressure levels, and a large span of the trailing edge was immersed in high fluctuating pressure levels. In the study of reference 5, the interaction of turbulence with the trailing edge of the flaps was considered to be the dominant noise source.

Other references (6 to 8) describe the existence of large orderly turbulence structures which are produced randomly at the nozzle lip and flow downstream. Reference 7 refers to them as ring or toroidal vortices. It is conceivable that, because of the macroscopic nature of these turbulence structures, they may interact with the flaps in an aerodynamic sense and result in unsteady inflow in the vicinity of the leading edges of the flaps. This unsteady inflow could cause a fluctuating lift response to an upwash disturbance, which in turn may have an influence on the production of noise.

The present study was conducted at the NASA Lewis Research Center to analyze noise data resulting from jet impingement near the trailing edge of a large flat plate (ref. 9) and a curved plate (ref. 2) for the purpose of obtaining a better understanding of the sources causing jet-flap interaction noise. Each plate approximated a semi-infinite surface with a jet exhaust impacting it near its trailing edge. The first objective of this analysis is to determine the contribution that trailing-edge noise makes in relation to the total jet-plate impingement noise for the test data of references 2 and 9. A theoretical and an empirical approach for calculating the noise level caused by the jet flow interaction with the trailing edge are discussed. Also, a method is presented by which the remaining impingement noise source levels may be approximated. These are then combined to provide a calculated estimate of the overall impingement noise level. The calculated noise levels (OASPL) are finally compared with the measured values of references 2 and 9. The second objective of this analysis is a consideration of investigations by Wagner (ref. 10) and Neuwerth (ref. 11) into the mechanisms that produce the peak value of the broadband SPL. An application of these mechanisms is made to the spectral data of references 2 and 9, permitting an estimation of the frequency at which the peak SPL value occurs.

A paper (ref. 12) based on the work presented in this report was given at the 87th meeting of the Acoustical Society of America in April 1974.

## ANALYSIS OF IMPINGEMENT NOISE

The primary objective of this report, in analyzing the data of references 2 and 9, is to determine the contribution that trailing-edge noise makes in relation to the total noise. In order to demonstrate this, it is necessary to estimate trailing-edge noise in relation

to the remaining noise sources. Reference 13 describes the principal contributing noise sources resulting from jet impingement on a solid surface to be jet mixing (i. e. , free shear-layer mixing over the surface), surface scrubbing, and edge noise. These noise sources are discussed in references 14, 15 and 16, and 17 and 18, respectively. In addition to these noise sources, Foss (ref. 19) discusses a noise source that may be produced by oblique jet impingement coupled with surface viscosity effects that result in surface vorticity fluctuations downstream of the impact point. Reference 19 suggests that a source of noise might arise from the vorticity effects of the flow field.

Figure 1(a) shows a jet impinging on a semi-infinite flat plate (having no leading edge) at an oblique angle. Imaginary surfaces  $A_1$ ,  $A_2$ , and  $A_3$ , after reference 20, are constructed within which the major volumes of surface noise sources are located. The surfaces include  $A_1$ , a spherical surface enclosing the impinging jet and the impingement region;  $A_2$ , a conical surface enclosing the wall jet; and  $A_3$ , a second spherical surface enclosing the flow region at the plate's trailing edge. These regions are presented to aid in depicting the hypothetical location of the jet impingement noise sources shown in figure 1(b). The noise sources included in figure 1(b) are those resulting from oblique jet impingement, surface scrubbing, trailing-edge interaction, and free shear-layer mixing over the deflected plate's surface. Unfortunately, of the indicated noise sources in figure 1(b), only edge noise may be expressed in an explicit mathematical form for the configuration shown. However, if it is assumed that in the impact and trailing-edge regions the sound sources are uncorrelated, their combined sound field may be approximated by superposition. Thus, the total overall sound pressure level (OASPL) is composed of the logarithmic sum of a trailing-edge OASPL and an impact OASPL. This summation is referred to herein as impingement noise:

$$(\text{OASPL})_{\text{impinge}} = 10 \log_{10} \left[ 10^{\frac{(\text{OASPL})_{\text{TE}}}{10}} + 10^{\frac{(\text{OASPL})_{\text{impact}}}{10}} \right] \quad (1)$$

Impact noise  $(\text{OASPL})_{\text{impact}}$  is defined as all the noise produced on a sufficiently large flat surface that excludes trailing-edge noise. This noise source would, therefore, be expected to include noise resulting from sources other than edge noise, that is, noise resulting from oblique jet impingement, surface scrubbing, and free-shear-layer mixing over the deflected plate's surface.

The following sections consist of, first, a review of two analytical methods used to estimate trailing-edge noise and, second, a method used to estimate impact noise.

## Trailing-Edge Noise

In both the theoretical approach (ref. 18) and the empirical approach (ref. 17) used to estimate trailing-edge noise, it is assumed that directed flow lies on the surface of a semi-infinite plane which is thin and rigid (fig. 2). The phenomena of interest occur near or at the edge of the half-plane labeled trailing edge in figure 2. Eddies, defined as regions of turbulence over which fluctuations of velocity are highly correlated, in the flow are well within a wavelength of the edge. The observer is assumed to be in the far field, and the flow region is turbulent and at high Reynolds number. As shown in figure 2,  $\delta$  represents the thickness of the boundary layer;  $W$  is taken as the spanwise length of the velocity profile between the centerline and a point where the local velocity is equal to one-half of the maximum velocity  $U_m$  of the free shear layer at the trailing edge;  $r$  is the distance to the observer measured from the trailing edge of the half-plane; and the angles  $\psi$  and  $\varphi$  locate, in cylindrical coordinates, the field point referenced to the plate's edge.

Theoretical approach. - The analysis of reference 18 is derived from Lighthill's analysis, in which the turbulence is divided into regions of perfect correlation where the size of each region is very much less than an acoustic wavelength. Such a region, shown in figure 3, occupies the space  $r_1 < r_0 < r_2$ ,  $\psi_1 < \psi_0 < \psi_2$ , and  $y_1 < y_0 < y_2$ . Also,  $\beta = \frac{1}{2}(\psi_1 + \psi_2)$  and  $\bar{r}_0 = \frac{1}{2}(r_1 + r_2)$ , where  $\bar{r}_0$  and  $\beta$  are regarded as the  $r_0, \psi_0$  cylindrical coordinates of the center of the eddy in relation to the edge of the half-plane. Equation (14) of reference 18 presents the acoustic intensity per unit eddy volume  $I$  in the following form, where the original symbols have been changed to the present nomenclature:

$$I = \frac{k^4 \sin \varphi \cos^2(\psi/2) \rho U_m^4 \alpha^2 V^2 \sin^2 \bar{\theta} \sin^2(\beta/2)}{\pi^3 c r^2 (k \bar{r}_0)^3} \quad (2)$$

The value of the normalized turbulence intensity  $\alpha$  generally varies between 0.01 and 0.2, and the gas properties are evaluated in the vicinity of the edge of the half-plane.

In reference 18 the lower bound of the correlation radius was evaluated as  $1.3 \delta$  for an eddy closely centered on the edge of the half-plane, where  $\delta$  is approximated by the thickness of the boundary layer at the edge of the half-plane. Equation (2) is simplified if  $\bar{r}_0$  is set equal to  $1.3 \delta$  and the following assumptions are made: First, the mean flow is directed normal to the trailing edge ( $\sin \bar{\theta} = 1$ ). Second, the field point lies in a plane perpendicular to both the half-plane and the plate's trailing edge ( $\sin \varphi = 1$ ). And third, the eddy is located at the half-plane's trailing edge ( $\sin \beta/2 = 1$ ). Thus, upon substitution equation (2) becomes

$$I = \frac{k\rho U_m^4 \alpha^2 V^2 \cos^2(\psi/2)}{\pi^3 c r^2 (1.3)^3 \delta^3} \quad (3)$$

In reference 18 the typical frequency of the source of the turbulence is considered to be of the order  $U_m/(2\delta)$  so that  $k$  is of the order  $(\pi U_m)/(\delta c)$ . Substituting into equation (3) and simplifying yield

$$I = \frac{\rho U_m^5 \alpha^2 V^2 \cos^2(\psi/2)}{21.68 c^2 r^2 \delta^4} \quad (4)$$

If, as in reference 18, the unit volume of the eddy  $V$  corresponds to the arbitrarily shaped region of perfect correlation shown in figure 3, then the volume may be approximated by setting

$$V = r_0(\psi_2 - \psi_1)(r_2 - r_1)(y_2 - y_1)$$

where  $r_0(\psi_2 - \psi_1)$ ,  $(r_2 - r_1)$ , and  $(y_2 - y_1)$  are very much less than an acoustic wavelength. The unit volume of the eddy then may reasonably be approximated by setting  $V = \delta^3$ . Substituting this unit volume term into equation (4) and simplifying the results yield the following expression for the acoustic intensity per unit eddy volume:

$$I = \frac{\rho U_m^5 \alpha^2 \delta^2 \cos^2(\psi/2)}{21.68 c^2 r^2} \quad (5)$$

The total intensity for the half-plane may be determined, as in reference 17, by assuming the effective wetted edge to have a total width of  $2W$  (fig. 2). Then the number  $N$  of unit sound sources (eddy volumes of radius  $\delta$ ) along it is determined from

$$N = \frac{W}{\delta} \quad (6)$$

and the total acoustic intensity is given by

$$I_{\text{tot}} = NI \quad (7)$$

Substituting equations (5) and (6) into equation (7) and simplifying give the total acoustic intensity as

$$I_{\text{tot}} = \frac{W \rho U_m^5 \alpha^2 \delta \cos^2(\psi/2)}{21.68 c^2 r^2} \quad (8)$$

Multiplying the rms acoustic intensity, equation (8), by  $\rho c$  results in the following form of the mean square sound pressure:

$$\bar{p}^2 = \frac{W \rho^2 U_m^5 \alpha^2 \delta \cos^2(\psi/2)}{21.68 c r^2} \quad (9)$$

The gas properties are evaluated at local conditions and the overall sound pressure level is given by

$$\text{OASPL} = 10 \log_{10} \left( \frac{\bar{p}}{P_{\text{ref}}} \right)^2 \quad (10)$$

where

$$P_{\text{ref}} = 2 \times 10^{-5} \text{ N/m}^2$$

Substituting equation (9) into equation (10), simplifying, and assuming  $\alpha = 0.1$  yield, in SI units,

$$\text{OASPL}_{\text{TE}} = 10 \log_{10} \left( \frac{W \delta U_m^5}{r^2} \right) + 10 \log_{10} \left[ \cos^2 \left( \frac{\psi}{2} \right) \right] + 10 \log_{10} \left( \frac{1.15 \times 10^6 \rho^2}{c} \right) \quad (11)$$

Empirical approach. - The equation for the OASPL distribution of trailing-edge noise taken from the empirically based derivation of Hayden (eq. (5) in ref. 17) is, in SI units,

$$\text{OASPL}_{\text{TE}} = 10 \log_{10} \left( \frac{W \delta U_m^6}{r^2} \right) + 10 \log_{10} \left[ \sin^2 \varphi \cos^2 \left( \frac{\psi}{2} \right) \right] + K \quad (12)$$



The constant  $K$  in equation (12) is an adjustment for the type of flow field that is assumed to exist near the plate's edge. In reference 21 the constant was determined experimentally for each of three possible flow regimes by Hayden and Chanaud using a plane turbulent wall jet flowing over a rigid flat plate. The flow regimes include, first, the potential core, where the wall shear layer beneath the laminar core behaves very much like a turbulent boundary layer ( $K = 17.45$ ); second, the two-dimensional or characteristic decay region, where the free shear layer has merged with the wall shear layer and the flow is in a fully developed turbulent state ( $K = 14.45$ ); and third, the radial decay region, where the side shear layers have merged and the flow field is fully three dimensional ( $K = 12.45$ ). For the conditions of the experimental data to be analyzed herein the flow field at the edge of the half-plane was assumed to be in the two-dimensional or characteristic decay regime as opposed to the radial decay regime. Therefore,  $K$  was set equal to 14.45. This choice is based in part on reference 22, which indicates that radial flow starts when the surface pressure gradient is nearly zero. Reference 23 presents flat-plate test data obtained at an oblique angle of  $60^\circ$  in which the surface pressure gradient is shown to approach zero at approximately 1.4 nozzle diameters downstream from the point where the nozzle axis intersects the plate. Because the trailing edge of each plate used in the tests of references 2 and 9 was located 1 nozzle diameter downstream from the intersection of the plate's surface by the jet axis, the flow at the plate's trailing edge is not considered to be in the radial decay regime. Therefore, the choice of the constant used ( $K = 14.45$ ) in equation (12) appears justified.

In comparing the exponents of the velocity  $U_m$  in equations (11) and (12) it should be noted that the sound intensity varies with the fifth and sixth powers, respectively.

### Impact Noise

In the absence of an explicit theoretical solution by which impact noise could be evaluated for the specific test configurations used in references 2 and 9, it is proposed instead that the test results of reference 24 be used to estimate this noise source. Reference 24 presents parametric test data of a jet exhaust impacting a large flat smooth board (2.4 m by 2.4 m). The resulting noise is isolated from leading- and trailing-edge noise but includes the remaining noise sources (i. e. , oblique jet impingement coupled with surface viscosity effects, surface scrubbing, and free shear-layer mixing over the deflected flat surface).

The test results of reference 24 are shown in figure 4 and were used in applications with references 2 and 9 (without the need for scaling modifications) because they were obtained under geometric and gas dynamic conditions similar to those of references 2 and 9. However, as noted in figure 4, only the range of data from  $0^\circ$  to  $120^\circ$  may be used to represent impact noise because at radiation angles  $\theta$  greater than  $120^\circ$  the

microphones were partially shielded by the board. Therefore, the data shown in figure 4 (ref. 24) are assumed to represent impact noise for radiation angles between  $0^{\circ}$  and  $120^{\circ}$  in the following application.

### Comparison of Calculated and Measured Impingement Noise Data

Equation (1), which represents the calculated total jet-plate impingement noise, is applied to two sets of experimental data: first, the flat-plate results of reference 9; and second, the curved-plate (slotless wing) data of reference 2, where the impingement flow field is assumed to approximate that over a flat plate. The total jet-plate impingement noise (eq. (1)) is composed of the logarithmic sum of a trailing-edge noise term and an impact noise term. In order to calculate trailing-edge noise by using equations (11) and (12), it is necessary to estimate the boundary layer height  $\delta$  and the spanwise wetted edge of the half-plate  $2W$ . Figures 5 and 6 present unpublished boundary layer and velocity profile data from the tests of reference 9. These data were used to evaluate  $\delta$  and  $W$  in the edge noise calculations made in the case of the flat plate. In the calculations made using equations (11) and (12) the angle  $\psi$  was determined graphically as a function of the acoustic radiation angle  $\theta$ . It may, however, be approximated by setting

$$\psi \approx 60 + \theta$$

Flat-plate data. - Figure 7 presents the flat-plate test setup used in reference 9. Sound data were taken at nozzle exit Mach numbers of 0.5, 0.7, and 0.9 along a 3.05-meter-radius microphone circle centered on the exit plane of the nozzle. The data were taken along an arc of the microphone circle from  $90^{\circ}$  to  $200^{\circ}$ , referenced to the upstream axis of the nozzle. The flat-plate OASPL data are plotted as a function of radiation angle in figure 8.

Figure 9 presents curves of OASPL as a function of radiation angles between  $0^{\circ}$  and  $120^{\circ}$ . The curves are restricted to this range because these are the limits of the useful data obtained in reference 24, which are used here to represent impact noise. In addition the range of the flat-plate test data shown in figure 9 is limited to the angles between  $90^{\circ}$  and  $120^{\circ}$ . However, these data include the location of greatest interest, which is directly below the plate ( $\theta = 90^{\circ}$ ). The large-flat-board data representing impact noise were taken from figure 4 after interpolation for the appropriate Mach numbers. The solid curve, labeled equation (1), represents the logarithmic summation of edge noise as calculated by using equation (12) and impact noise as approximated from the experimental data of reference 24. Although the span of the overlap is small for the solid curve and the flat-plate data, the agreement is good except at  $120^{\circ}$ , which is probably due to the shielding effect of the large board.

Also shown in figure 9 are the curves determined by using equation (11), which is based on the theory of reference 18, and by using equation (12), which is based on the empirical relation of reference 17. A comparison of these curves with the flat-plate data of reference 9 shows clear disagreement. Therefore, edge noise as predicted by the methods of references 17 and 18 does not appear to be the dominant source of noise at radiation angles between  $90^\circ$  and  $120^\circ$  for the conditions at which the flat plate was tested.

A comparison of figures 9(a), (b), and (c) indicates that impact noise becomes more dominant over edge noise as the jet Mach number increases from 0.5 to 0.9. At  $M_j = 0.5$  (fig. 9(a)) a comparison of the curves representing trailing-edge noise and impact noise indicates that impact noise is dominant in the region between radiation angles of  $80^\circ$  and at least  $105^\circ$ . In order to verify this, the velocity exponent was investigated as a function of the radiation angle around the microphone circle. The results are shown in the lower portion of figures 9(a), (b), and (c). In the region from  $90^\circ$  to  $105^\circ$ , the velocity varied to nominally the 8th power in figures 9(a) and (b) and to the 12th power in figure 9(c). This agrees with the results of reference 24, which show that an 8th-power curve of the velocity fits the data between nozzle exit Mach numbers of approximately 0.4 and 0.7, and a gradually higher power is required at higher Mach numbers. Specifically, at a Mach number of 0.9 a 12th-power curve approximates the data.

The increase in the velocity exponent at the highest Mach number of 0.9 may be an indication of the existence of one of the surface impingement phenomena described by Powell (ref. 15). Powell describes the degeneration of quadrupoles ( $U^8$  dependence) into octupole sound generators ( $U^{10}$  dependence) as flow at high Reynolds number increases to still higher Reynolds number for the case of a plane infinite surface supporting a finite turbulent boundary layer. The quadrupoles involved in this phenomenon are those lateral quadrupoles of the type that would be associated with fluctuations across the shear of an adjacent boundary layer. Reference 15 indicates that at low speeds the octupole power cannot amount to much. However, at high speeds and for "thicker" flows it may be of some importance. The mechanism by which the fluctuations take place across the shear of an adjacent boundary layer may be described by Foss's discussion of oblique jet impingement in reference 25. He notes that vorticity considerations account for the observed behavior of the jet flow field in the impingement region and these allow the surface pressure gradients to be interpreted as sources of vorticity. Also reference 25 indicates that the resulting concentrated motion in the region near the wall produces substantial domains over which these velocity or vorticity fluctuations are correlated.

Curved-plate data. - Figure 10 presents the test setup of the curved plate, or slotless wing as it is referred to in reference 2, in the EBF STOL approach condition. The leading edge of the curved plate is well outside the jet flow, and the intersection of the jet axis with the plate is located 1 diameter upstream from its trailing edge and 7 nozzle diameters downstream from the nozzle exit plate. Also, the trailing edge is oriented so

that the included angle between a tangent to it and the jet axis is  $60^\circ$ . Thus, the orientation of the curved plate to the jet stream and nozzle exit is the same as that of the flat plate (ref. 9) shown in figure 7.

Figure 11 presents OASPL data from reference 2 for the curved plate. The empirical relation for edge noise (eq. (12)) and the large-flat-board impact noise results of reference 24 are also shown. These were summed by using equation (1) and resulted in the solid curve. A boundary layer thickness of 0.64 centimeter (ref. 2, fig. 24) was used in the calculations made for edge noise. The data of reference 2 show good agreement with the solid curve with the exceptions at radiation angles of  $0^\circ$  and  $120^\circ$ , which are probably caused by the shielding effects of the nozzle and large board, respectively. In addition, reference 2 notes that the exponent of the velocity varied with radiation angle along the microphone circle. For example, the OASPL was found to vary as  $U_j^6$  at a radiation angle of  $60^\circ$ , but at  $100^\circ$  it varied as  $U_j^8$ . Comparing this result with the curves representing the large-flat-board data (impact noise) and edge noise at  $60^\circ$  and  $100^\circ$  indicates that this result would be expected on the basis of the present analysis.

## PREDICTION OF PEAK SOUND-PRESSURE-LEVEL FREQUENCY

In this section the second objective of this report is considered, namely, the mechanism producing the peak value of the broadband SPL and an application of the mechanism to the spectral data of references 2 and 9.

Studies of the mechanism producing the peak value of SPL resulting from jet impingement on a flat surface were made in references 10 and 11. In both studies the large-scale, ordered structure of the jet was considered to be the prime factor in establishing the frequency associated with the peak SPL value. In the following sections, the nature of the large-scale, ordered structure of a free jet is discussed, followed by a consideration of the feedback interaction of this type of flow structure with a surface. Finally, a comparison is made between the frequencies of generation of several proposed modal forms of the large-scale, ordered structures and the frequencies at which the peak values of the measured spectral data of references 2 and 9 occurred.

### Theory

Conical free jet. - Free-jet studies (refs. 6 to 8, and 11) suggest that there is a large-scale, ordered structure in the shear layer surrounding the jet core. The structure can be observed in low-speed jets (ref. 8), as a sequence of toroidal vortices formed 1 to 2 diameters downstream from the nozzle lip, and persists downstream. The vortical structure is described as a large-scale component of the shear-layer turbulence

that is highly correlated over distances comparable to the thickness of the mixing layer. In reference 7, this structure was modeled as an axisymmetric train of toroidal vortices, and it was shown that the main noise production occurs within the first few diameters downstream of the jet exhaust plane and is primarily due to temporal changes in the toroidal radii. The production of the structure is implicated as an important contributor to high-frequency jet noise.

Reference 11 describes an axisymmetric structure in a free subsonic jet flow which appears to be periodic and travels downstream with a convection speed of 0.63 of the jet exit velocity. Figure 12, taken from reference 11, shows several experimentally determined curves of Strouhal number based on the frequency  $f_s$  of the structure's appearance as a function of jet Mach number. These curves describe three modes that the structure appears to operate in. First, an axisymmetric vortex or fundamental mode is shown for jet Mach numbers below 0.85. Second, a mode referred to as the first azimuthal mode can only be observed at jet Mach numbers between 0.85 and 1.0. In this case the natural orderly structure has the form of a helix about the jet flow. Third, measurements indicate that the axisymmetric vortex mode has a first harmonic, which is also shown. Finally, figure 12 indicates that the three modes of operation show a decrease in Strouhal number with increasing Mach number. It is noted in reference 11 that, even if the structures are very weak, they are effective noise sources because the quadrupoles within them are fluctuating in a coherent manner and the structures extend over the whole noise-producing region of the jet.

Planar parallel flow. - It is noted in reference 10 that in tests using axially symmetric free jets of low velocity, the free boundary layer of the jet can only be excited into ring vortex formation by acoustic effects within a limited frequency band, and that the intensity of the excitation was found to depend on the Strouhal number  $S = f_s \xi / U$ , where  $\xi$  is defined as the momentum thickness (pulse loss thickness, ref. 10) of the free boundary (or shear) layer. This effect suggested that the frequency of vortical formation may be theoretically estimated by applying free-boundary-layer instability theory to jet flow. The dependence of the amplification factor (spatial regeneration factor, ref. 10) of the free boundary layer of a planar parallel flow on the Strouhal number has been calculated for compressible media in reference 26 (referred to in ref. 10). Reference 26 is a study of the instability of the free boundary layers of planar parallel flows. Parametric curves based on the theoretical study of reference 26 are presented in reference 10 and are plotted in the form of amplification factor as a function of Strouhal number for several Mach numbers. Thus, the frequency of vortical formation of a circular jet flow can be determined if it is assumed, first, that the free-boundary-layer instability theory for planar parallel flow (ref. 26) is applicable to circular jet flow (conical flow) and, second, that the frequency of vortical formation  $f_s$  (which occurs at resonant instability of a circular jet flow) is identical to the frequency  $f_p$  at which the

peak value of the amplification factor occurs in the theoretical amplification curves from reference 26.

In order to use the amplification curves appearing in reference 10 (taken from ref. 26), the term  $\xi$  in the Strouhal number must be evaluated for the case of a circular jet flow. An experiment was performed (ref. 10) to determine an expression for  $\xi$  for the tested circular-nozzle-to-flat-plate-surface separation distances. It was found to take the following form:

$$\xi = 0.0214 D$$

Figure 13 is a plot of the Strouhal numbers corresponding to the peak values of the amplification factors as a function of Mach number, based on the curves presented in reference 10. The Strouhal number is based on the frequency  $f_p$  at which the peak value of the amplification factor occurs and on the nozzle exit velocity  $U_j$ . It is assumed here that the frequency  $f_p$  equals the frequency  $f_s$  of vortical formation of a circular jet flow. Thus, from figure 13 the resonant frequency of vortical formation for a free jet can be predicted.

Jet surface interaction. - The effect of the impingement of a vortical-structured jet on a solid surface is discussed in references 10 and 11. In reference 10, as a result of experimental observation of jet impingement, it is hypothesized that, in the free boundary layer near the exit of a circular nozzle, ring vortices are formed periodically with suitable excitation by a winding-up process of the boundary layer. The vortices flow downstream in intervals while absorbing energy and cause periodic pressure variations in the dynamic pressure head of the jet core upon impacting the flat surface. These pressure variations propagate in part externally in the form of sound wave and in part internally as periodic pressure interferences against the flow direction. The periodic pressure interferences upon reaching the nozzle outlet cause the formation periodically of new ring vortices due to feedback of the back-pressure wave.

With the aid of schlieren imagery, reference 10 indicates that the periodic formation of ring vortices at the edge of the jet and a standing wave of alternating pressure in the area bounded by the ring vortices of the jet were only present if the distance between the surface and the nozzle exit did not exceed 5 to 6 diameters and the Mach number of the jet was greater than 0.55. The frequency of vortical formation and release was found to be synchronous with the frequency of the periodic pressure variations at the impact surface.

Reference 11 is an extension of the work in reference 10, with particular emphasis on an optical investigation in which high-speed spark-schlieren photographs of the flow field were obtained. In reference 11 it is indicated that the feedback reinforces the first harmonic of the axisymmetric mode of the natural turbulence structure of the jet, which is then described as giving rise to ring vortices. The reflected wave from the solid

surface propagates upstream as an oblique wave to the jet axis and is totally reflected at the jet boundary layer. Thus, the acoustic feedback wave moving upstream inside the jet core region effects a reinforcement of the natural pulsation of the jet and thus a reinforcement of the natural axisymmetric turbulence structure. New strong ring vortices are formed, and the feedback loop is closed. Reference 11 indicates that the spectrum of the radiated sound has a peak at the frequency of the ring vortices. In figure 14, taken from reference 11, the experimentally determined variation of the Strouhal number for the case of acoustic feedback is presented as a function of jet Mach number. At jet Mach numbers below 0.5 the feedback phenomenon disappears; however, the natural structure of turbulence is still present. The preceding flow phenomena, considered in reference 11, occur only for nozzle-to-impact-surface distances of less than 6 nozzle diameters.

In references 6 to 8 and 11 it was found that the toroidal (or ring) vortices described in reference 10 are also present in free jets; therefore, their existence does not depend only on jet impingement on a surface located within 6 nozzle diameters of the jet exit, as indicated in reference 10. The lack of their observation in reference 10 was most probably due to the insensitivity of the schlieren system used in the experiments. It appears that the jet structure observed in reference 10, in the impingement experiments, was really a reinforced ring vortex or vortex wave.

#### Application to Test Data

In this section the prediction techniques of references 10 and 11 are applied to the spectral data from references 2 (curved plate) and 9 (flat plate). Figures 15 and 16 present the broadband spectral distributions of the sound pressure level (SPL) for the flat plate of reference 9 and the curved plate of reference 2, respectively. The SPL data were taken with a 1.27-centimeter-diameter condenser microphone and have not been corrected for ground reflection cancellations and reinforcements, which are denoted by  $C_i$  and  $R_i$ , respectively, in the figures.

The flat-plate spectral data (fig. 15) were taken only at a radiation angle of  $93^\circ$  and at nozzle exit Mach numbers of 0.5, 0.7, and 0.9 over a gravel-covered surface. Four different tick marks are distributed along each curve and denote the various possible modes of operation represented by the curves in figures 12 to 14. The tick mark labeled ① represents the experimentally based fundamental axisymmetric vortex mode (applicable at  $M_j < 0.85$ ) of the naturally orderly structure of turbulence calculated by using the appropriate curve of figure 12. The tick mark labeled ② is its first azimuthal (or helical) mode (applicable for  $M_j \geq 0.85$ , ref. 11). The tick mark labeled ③ represents the first harmonic of the axisymmetric vortex mode. The tick mark labeled ④ represents the planar-parallel-flow boundary-layer instability mode calculated by using the

curve of figure 13. The tick mark labeled (5) represents the frequency at which the reinforced axisymmetric vortex mode operates with acoustic feedback. Tick mark (5), calculated by using figure 14, was included for completeness even though the location of the flat plate (also the curved plate) was 7 nozzle diameters downstream from the nozzle exit plane, probably making the feedback phenomenon inoperative. Comparison of the tick marks with the spectra of the flat plate indicates that the first harmonic of the axisymmetric vortex mode (3) and the planar -parallel-flow boundary-layer -instability vortex mode (4) correspond most closely to the peak SPL value of the spectra. A comparison of the trend of the data with modes (3) and (4) as a function of jet Mach number is considered good.

The curved-plate data shown in figure 16 were taken over a smooth concrete surface at a radiation angle of  $80^\circ$  as part of the study reported in reference 2 but have not been published previously. (No data were taken in the vicinity of  $90^\circ$ .) The data were obtained at jet Mach numbers of 0.57 and 0.92. Comparison of the tick marks with the spectra indicate once again that vortex modes (3) and (4) most nearly correspond to the peak SPL values. A comparison of the trend of the data with modes (3) and (4) as a function of jet Mach number is considered good.

Figures 15 and 16 indicate that the modes tend to operate over a smaller span in frequency as the jet velocity is increased. Thus, they would tend to reinforce each other with increasing jet velocity if they were simultaneously active.

### Implications of Results

The apparent agreement between theory and experiment may indicate that the mechanisms hypothesized in references 10 and 11 were operating in the tests of references 2 and 9. As a consequence, any technique which inhibits the production or growth of the toroidal structures may produce noise suppression. One method which might be applied to suppress the flat-plate noise would be to move the nozzle to within 1 or 2 nozzle diameters of the plate. Although this would produce acoustic feedback, the feedback can apparently be suppressed, as suggested in references 10 and 11. The advantages of this might be, first, a reduction in magnitude of the large and wide-spread unsteady surface-pressure fluctuations caused by the fully developed ring vortices; second, exposure of the flat plate to the finer turbulence of the nozzle's core flow, which reference 11 implies would result in reducing the high-frequency components of the jet noise; and third, increased shielding by the flat plate of the rearward quadrant beneath the nozzle and plate from the high-frequency noise. Because, in the second instance, more of the flat plate's surface would be submerged in a much finer turbulence flow, it is likely that the application of noise suppression devices to the flat plate and/or its trailing edge would be



more effective. Possible disadvantages of this method include changes in the lift distribution over the wing-flap combination, high surface temperatures that could result from a more focused and less diffused jet impingement of the flaps' surfaces, and engine back-pressure effects producing instability in mass flow rate.

### CONCLUDING REMARKS

An available theory and recent experimental data have been used in an analytical relation which approximates the sound-field directivity data obtained from a subsonic cold gas jet impacting a flat plate in the vicinity of its trailing edge. The method applies over an arc of approximately  $105^\circ$  and was devised by assuming that two uncorrelated sound sources (i. e. , impact noise and edge noise) are active in the vicinity of the flat plate's trailing edge. The agreement between the analytical expression and two independent sets of data is considered good. The results of the analysis indicate that the noise from the plate emanates from two principal sources: the impact of the jet on the plate's surface, and the flow over the trailing edge of the plate. It appears that the dominant source of noise produced at jet Mach numbers above 0.5 and heard "beneath" the nozzle and flat plate (in the sense of an aircraft flyover) is impact noise ( $U^8$  dependence) rather than edge noise ( $U^5$  or  $U^6$  dependence). The dominance of impact noise over edge noise was found to increase with increasing jet Mach number.

The small (approximately 2.5 dB) reductions in noise level obtained in recent attempts to suppress noise produced in the vicinity of the trailing edge of a flat plate using edge-blowing techniques (ref. 9) may be explained by the dominance of impact noise over edge noise.

The jet-plate impingement work presented herein implies that the dominant noise produced beneath EBF STOL aircraft for jet Mach numbers above 0.5 may not be caused by edge noise emanating from the trailing edge of the last flap. Rather, it may be the result of the jet impacting the flap and/or unsteady inflow in the vicinity of the leading edge of the flap, resulting in a possible fluctuating lift response to an upwash disturbance.

The peak value of the broadband sound spectral distribution appears to be governed by a phenomenon which produces periodic formation and shedding of ring vortices from the outlet of the nozzle. Test data compare favorably with theory in magnitude and trend. This result suggests that noise suppression may result if the production or growth of these toroidal structures is inhibited.

Since the mechanisms producing noise are basically fluid dynamic phenomena, there is an increasing need for surface and boundary layer aerodynamic data in conjunction with detailed acoustic experimentation on flap and impingement noise.

Lewis Research Center,  
National Aeronautics and Space Administration,  
Cleveland, Ohio, October 3, 1974,  
505-03.

## APPENDIX - SYMBOLS

$A_1, A_2, A_3$	imaginary surfaces within which noise sources are located over flat-plate surface
$C_i (i=2, 3, 4)$	ground reflection cancellations
$c$	speed of sound
$D$	nozzle exit diameter
$f_p$	frequency, dependent on peak value of amplification factor for planar parallel flow
$f_s$	frequency of appearance of large turbulent structure for circular jet flow
$I$	sound intensity
$K$	constant
$k$	wave number
$M$	<i>Mach number of stream</i>
$N$	number of eddy volumes along trailing edge
$\bar{P}^2$	mean square sound pressure
$P_{ref}$	reference sound pressure
$R_i (i=2, 3, 4)$	ground reflection reinforcements
$r$	distance between observer and trailing edge
$\bar{r}_0, r_0$	equivalent radial coordinates of center of an eddy referenced to trailing edge
$S$	Strouhal number
$U$	mean velocity of stream (isentropic expansion velocity)
$U_m$	maximum mean velocity of free shear layer at trailing edge
$V$	volume of an eddy
$W$	half spanwise width of velocity profile between points where local velocity is equal to $1/2 U_m$ at trailing edge
$x, y, z, z'$	Cartesian coordinate system (figs. 2, 7, or 10)
$\alpha$	normalized turbulence intensity
$\beta, \psi_0$	equivalent cylindrical coordinate of center of an eddy referenced to trailing edge
$\delta$	thickness of boundary layer; radius of eddy volume
$\theta$	radiation angle measured from nozzle inlet axis (fig. 7 or 10)

$\bar{\theta}$       angle mean flow makes with trailing edge  
 $\xi$       momentum thickness (pulse loss thickness)  
 $\rho$       density of undisturbed fluid  
 $\varphi, \psi$     shown in figure 2 or 3

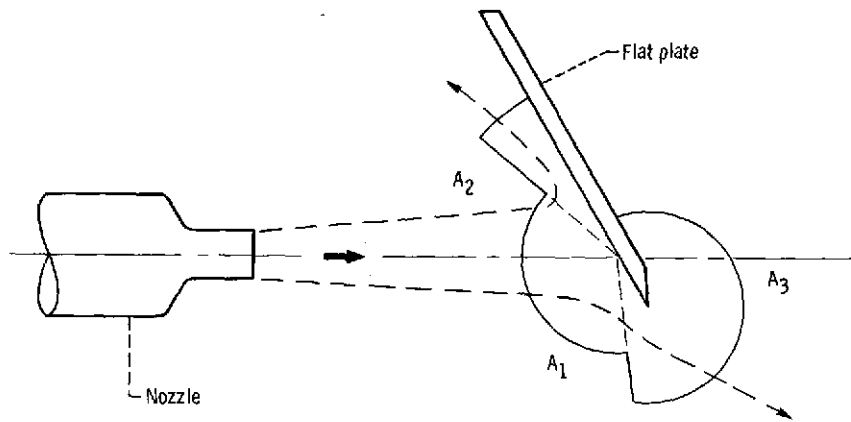
Subscripts:

impact    impact  
impinge    impingement  
j          jet exit condition  
ref        reference  
TE        trailing edge  
tot        total  
0          center  
1          point 1  
2          point 2

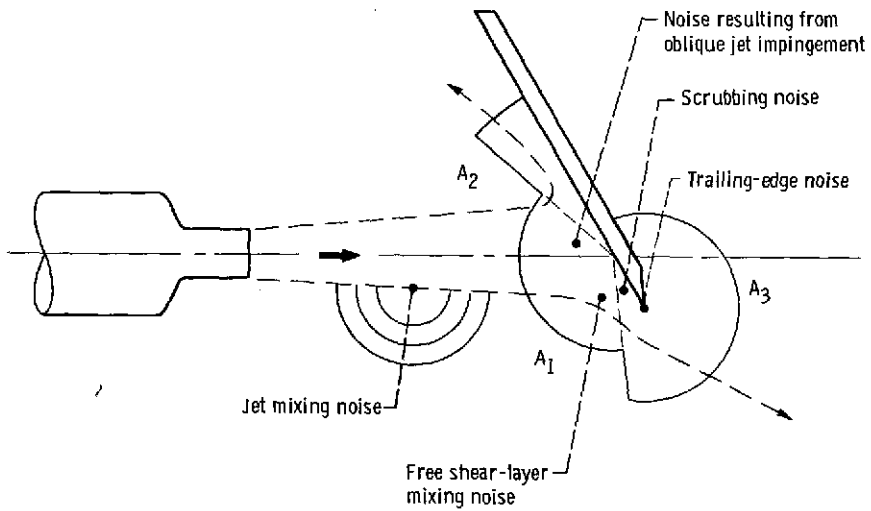
## REFERENCES

1. Dorsch, Robert G. ; Kreim, Walter J. ; and Olsen, William A. : Externally-Blown-Flap Noise. AIAA Paper 72-129, Jan. 1972.
2. Olsen, William A. ; Dorsch, Robert G. ; and Miles, Jeffrey H. : Noise Produced by a Small-Scale, Externally Blown Flap. NASA TN D-6636, 1972.
3. Dorsch, R. G. ; Lasagna, P. L. ; Maglieri, D. J. ; and Olsen, W. A. : Flap Noise. Aircraft Engine Noise Reduction. NASA SP-311, 1972, pp. 259-290.
4. Dorsch, R. G. ; Goodykoontz, J. H. ; and Sargent, N. B. : Effect of Configuration Variation on Externally Blown Flap Noise. AIAA Paper 74-190, Jan. -Feb. 1974.
5. Hayden, Richard E. ; Kadman, Yoram ; and Chanaud, Robert C. : A Study of the Variable Impedance Surface Concept as a Means for Reducing Noise from Jet Interaction with Developed Lift-Augmenting Flaps. (Rept. -2399, Bolt, Beranek and Newman, Inc.) Available as NASA CR-112166, 1972.
6. Wooten, D. C. ; Wooldridge, C. E. ; and Amaro, A. J. : The Structure of Jet Turbulence Producing Jet Noise. (Stanford Research Inst.) Available as NASA CR-126483, 1971.
7. Hardin, Jay C. : Analysis of Noise Produced by an Orderly Structure of Turbulent Jets. NASA TN D-7242, 1973.
8. Crow, S. C. ; and Champagne, F. H. : Orderly Structure in Jet Turbulence. J. Fluid Mech., vol. 48, Aug. 16, 1971, pp. 547-591.
9. McKinzie, D. J., Jr. ; and Burns, R. J. : Externally Blown Flap Trailing Edge Noise Reduction by Slot Blowing - A Preliminary Study. AIAA Paper 73-245, 1973.
10. Wagner, F. R. : The Sound and Flow Field of an Axially Symmetric Free Jet Upon Impact on a Wall. Z. Flugwiss., vol. 19, no. 1, Jan. 1971, pp. 30-44.
11. Neuwerth, G. : Acoustic Feedback Phenomena of the Subsonic and Hypersonic Free Jet Impinging on a Foreign Body. NASA TT F-15719, 1974.
12. McKinzie, D. J., Jr. ; and Burns, R. J. : Analysis of Noise Produced by Jet Impact Near the Trailing Edge of a Flat Plate. Paper JJ5 Acous. Soc. Am., April 1974.
13. Powell, Alan: Theory and Experiment in Aerodynamic Noise, with a Critique on Research on Jet Flows in Their Relationship to Sound. Second Symposium on Naval Hydrodynamics, Ralph D. Cooper, ed., National Academy of Sciences - National Research Council, 1958, pp. 1-27.
14. Ribner, H. S. : Jets and Noise. Canadian Aero. Space J., vol. 14, no. 8, Oct. 1968, pp. 281-298.

15. Powell, Alan: Aerodynamic Noise and the Plane Boundary. *J. Acous. Soc. Am.*, vol. 32, no. 8, Aug. 1960, pp. 982-990.
16. Lotsch, H. K. V.: On Pseudo-Sound in a Plane Turbulent Boundary-Layer Turbulence. *Bull. Amer. Phys. Soc.*, vol. 16, no. 11, Nov. 1971, pp. 1323-1324.
17. Hayden, Richard E.: Noise from Interaction of Flow With Rigid Surfaces: A Review of Current Status of Prediction Techniques. NASA CR-2126, Oct. 1972.
18. Ffowcs Williams, J. E.; and Hall, L. H.: Aerodynamic Sound Generation by Turbulent Flow in the Vicinity of a Scattering Half Plane. *J. Fluid Mech.*, vol. 40, pt. 4, Mar. 9, 1970, pp. 657-670.
19. Foss, John F.; and Kleis, Stanley J.: The Oblique Impingement of an Axisymmetric Jet. Division of Engineering Research, Michigan State Univ., 1972.
20. Pan, Y. S.: Cross-Correlation Methods for Studying Near- and Far-Field Noise Characteristics of Several Flow-Surface Interaction Problems. Paper G10, *Acous. Soc. Am.*, April 1974.
21. Hayden, R. E.; and Chanaud, R. C.: Sound Generation by Turbulent Wall Jet Flow Over a Trailing Edge. Paper FF-10, *Acous. Soc. Am.*, April 1970.
22. Gauntner, James W.; Livingood, John N. B.; and Hrycak, Peter: Survey of Literature on Flow Characteristics of a Single Turbulent Jet Impinging on a Flat Plate. NASA TN D-5652, 1970.
23. Donaldson, Coleman DuP.; and Snedeker, Richard S.: A Study of Free Jet Impingement. Part 1 - Mean Properties of Free and Impinging Jets. *J. Fluid Mech.*, vol. 45, pt. 2, Jan. 30, 1971, pp. 281-320.
24. Olsen, William A.; Miles, Jeffrey H.; and Dorsch, Robert G.: Noise Generated by Impingement of a Jet Upon a Large Flat Board. NASA TN D-7075, 1972.
25. Foss, John F.: Vorticity Effects in Oblique Jet Impingement Flows as Background for the Acoustics Problem. Interagency Symposium on University Research in Transportation Noise, vol. 1, Stanford Univ., Stanford, Calif., March 28 - 30, 1973, pp. 273-288.
26. Gropengiesser, Hans: Study of the Stability of Boundary Layers and Compressible Fluids. NASA TT F-12786, 1969.



(a) Noise regions.



(b) Noise sources.

Figure 1. - Jet impinging on semi-infinite flat plate.

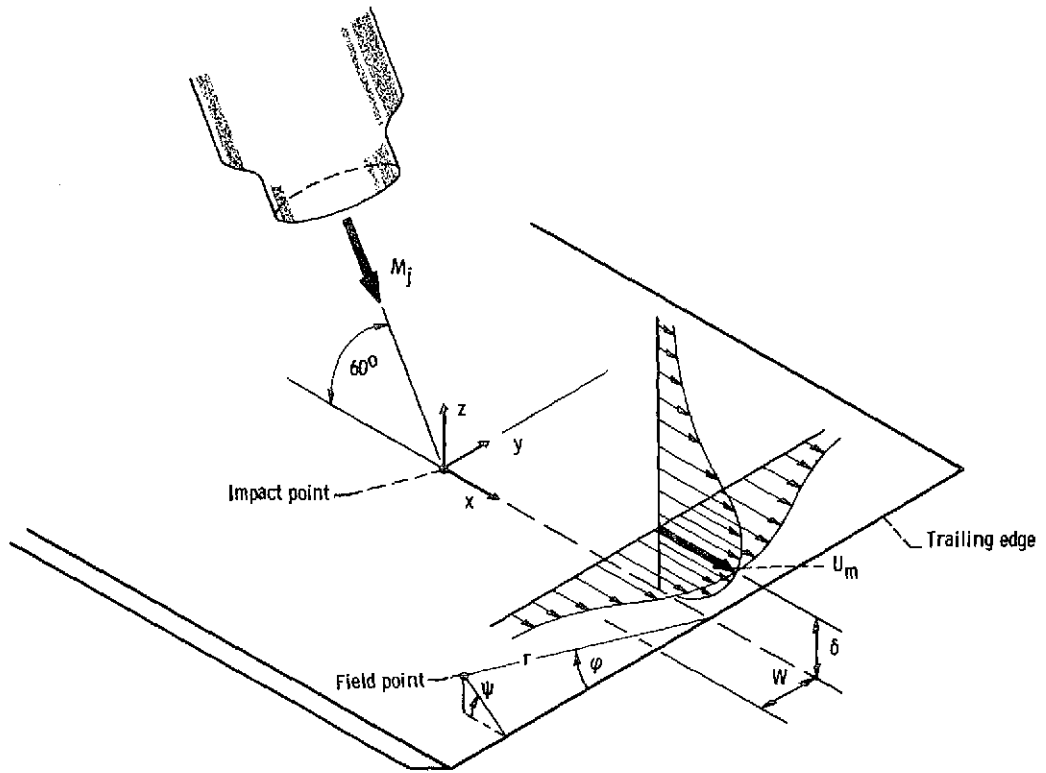


Figure 2. - Coordinate system of a jet impinging on a semi-infinite half plane near its trailing edge.



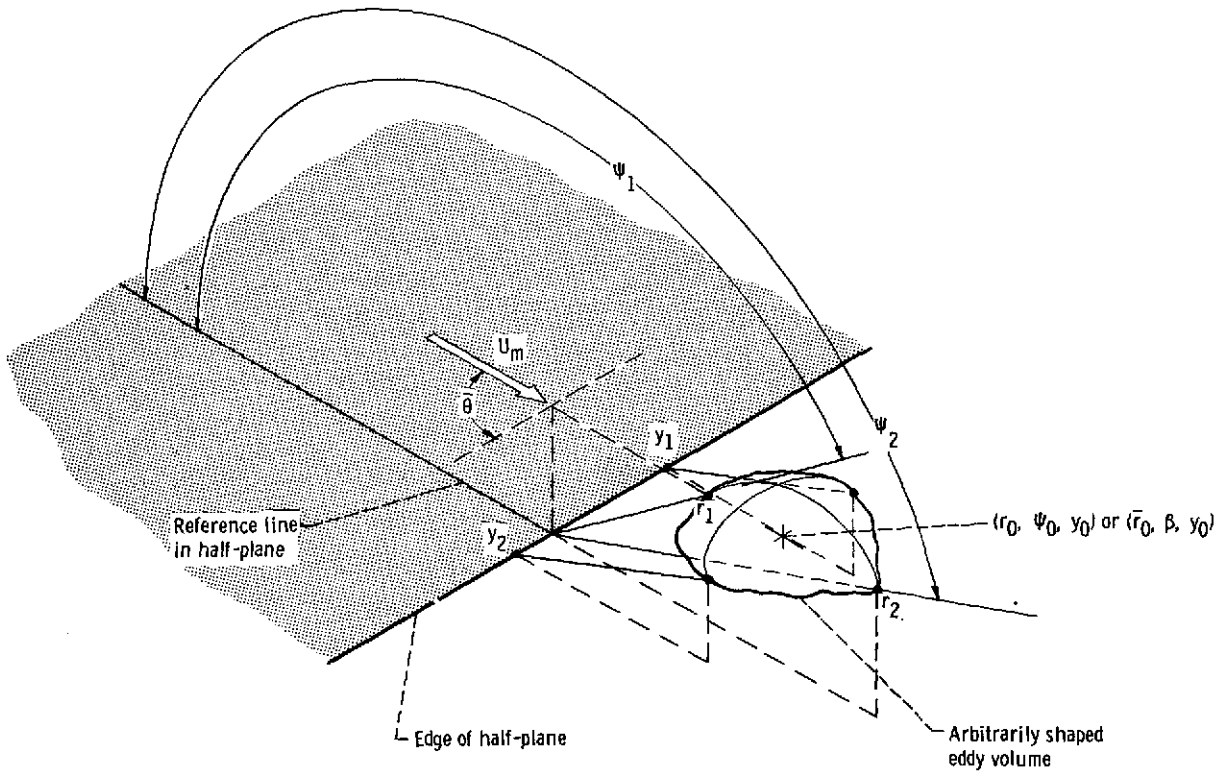


Figure 3. - Cylindrical coordinate system of directed flow lying on surface of semi-infinite plane.

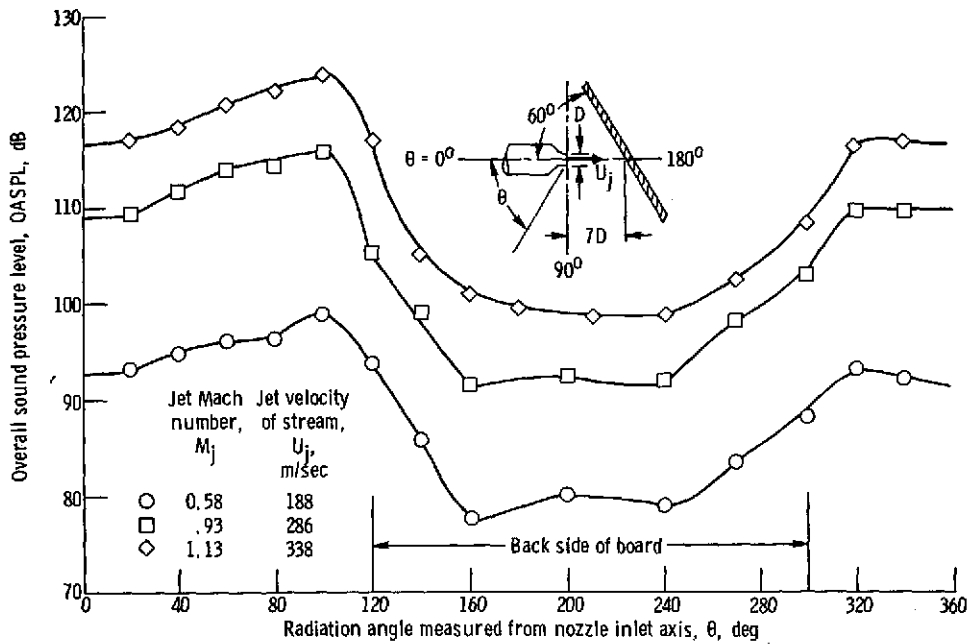


Figure 4. - Overall sound-pressure-level distribution for large flat board. Nozzle exit diameter,  $D$ , 5.2 centimeters; azimuthal angle,  $0^\circ$ . (From ref. 24.)

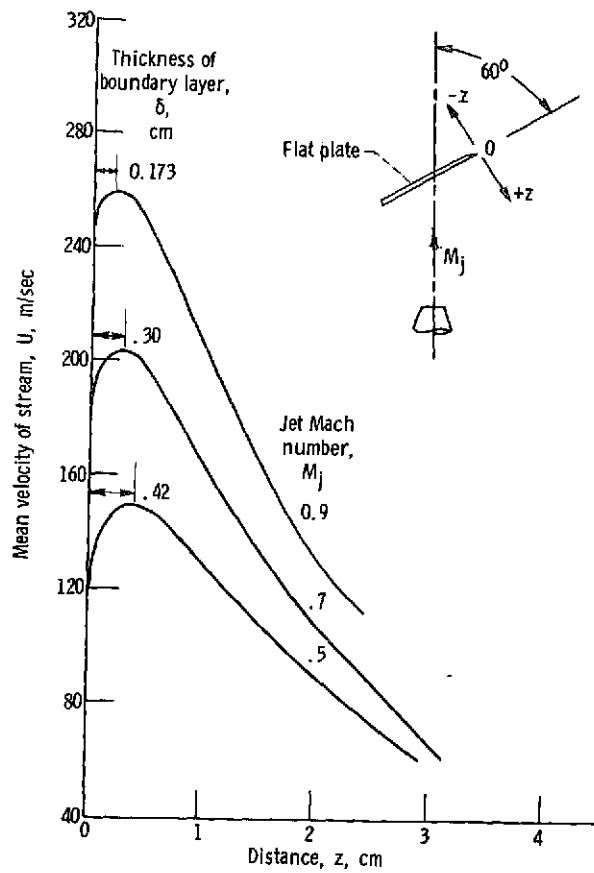


Figure 5. - Velocity profiles in z-direction at trailing edge of flat plate.  $z'/D = 7$ .

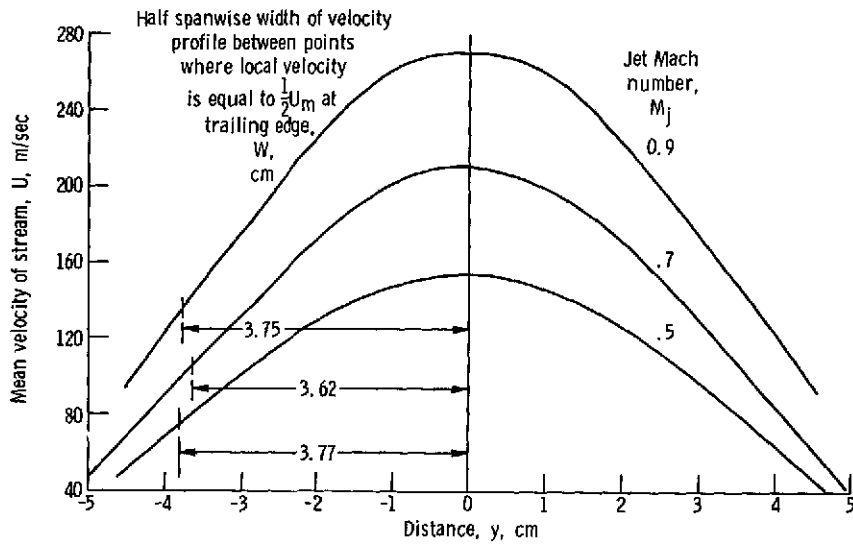


Figure 6. - Typical spanwise velocity profiles at trailing edge and 1.1 centimeter above flat plate.  $z'/D = 7$ .

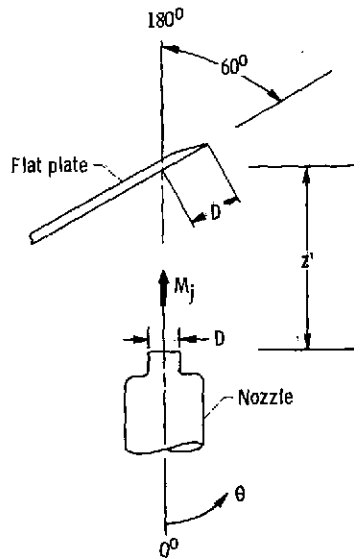


Figure 7. - Overhead view of flat-plate test setup used in reference 9. Nozzle exit diameter,  $D$ , 5.08 centimeters;  $z'/D = 7$ .

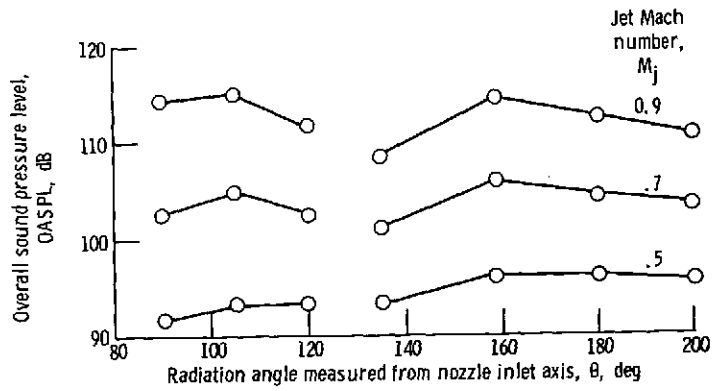


Figure 8. - Overall sound-pressure-level distribution for flat plate at  $z'/D = 7$ . (From ref. 9.)

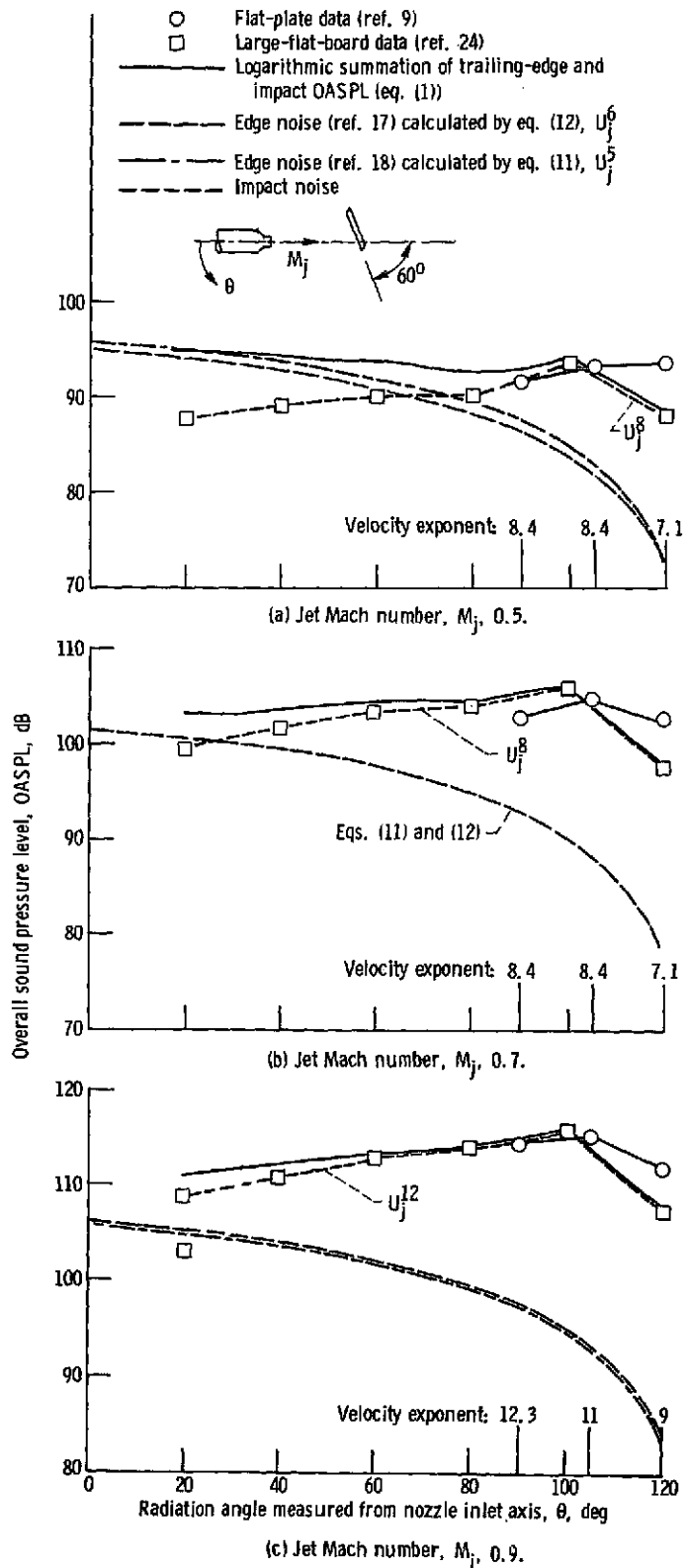


Figure 9. - Comparison of calculated impact noise and edge noise with measured flat-plate data.

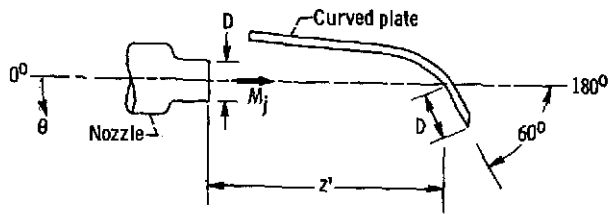


Figure 10. - Overhead view of curved-plate test setup used in reference 2. Nozzle exit diameter,  $D$ , 5.08 centimeters;  $z'/D = 7$ .

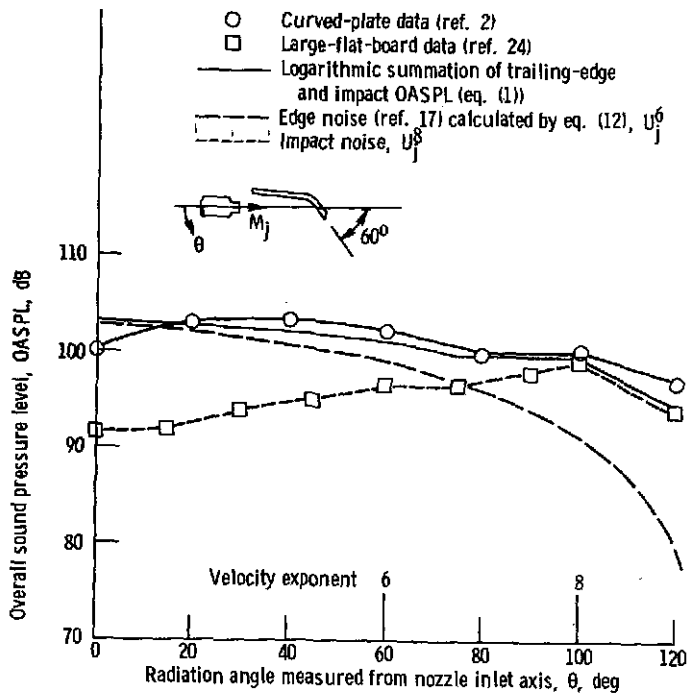


Figure 11. - Comparison of calculated impact noise and edge noise with measured curved-plate data. Jet Mach number,  $M_j$ , 0.57.

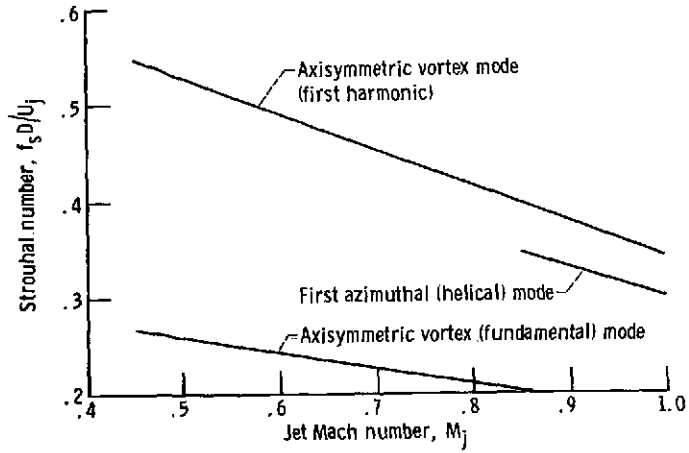


Figure 12. - Measured Strouhal numbers of natural orderly structure of turbulence of cold-flow circular free jet flow. (From ref. 11.)

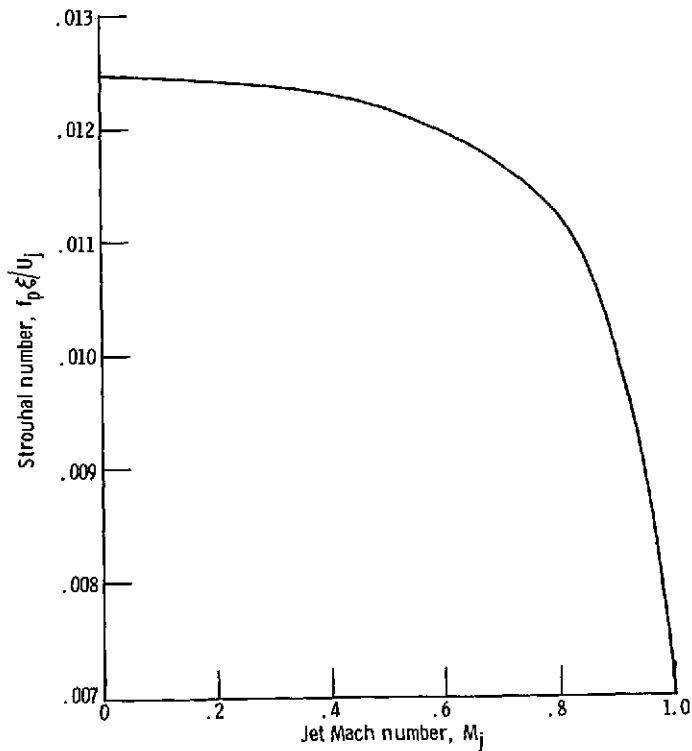


Figure 13. - Theoretical Strouhal number of peak values of amplification factors for free planar parallel flow, based on amplification curves from reference 26 assuming adiabatic conditions.

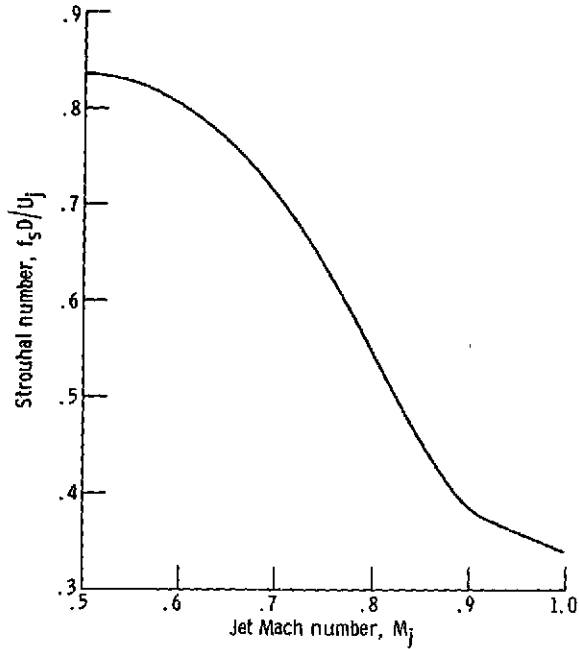


Figure 14. - Experimental Strouhal number of cold-flow circular jet with acoustic feedback. (From ref. 11.)

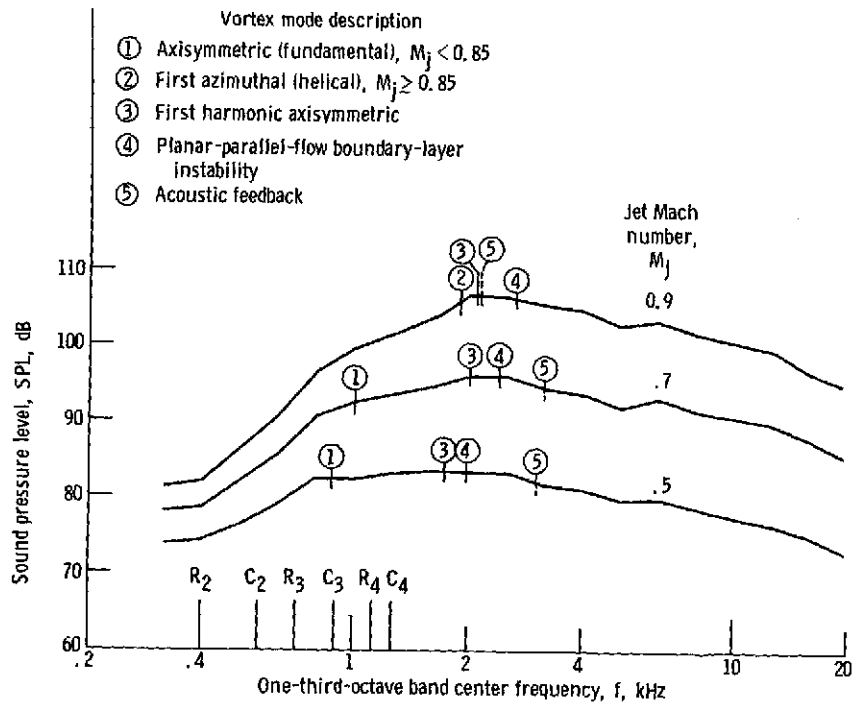


Figure 15. - Sound-pressure-level spectra for flat plate at radiation angle of  $93^\circ$ , showing boundary layer instability modes of orderly structure of jet turbulence.

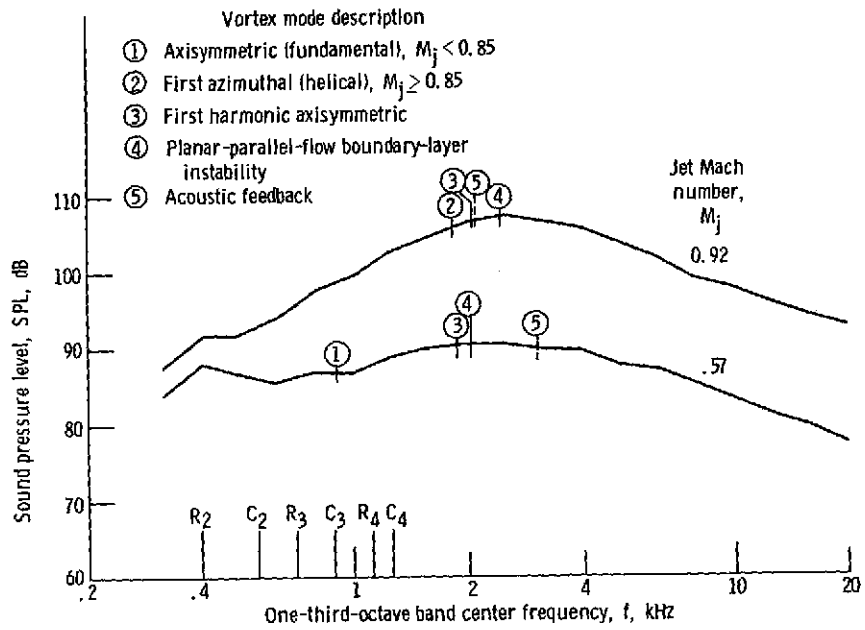


Figure 16. - Sound-pressure-level spectra for curved plate at radiation angle of  $80^\circ$ , showing boundary layer instability modes of orderly structure of jet turbulence.